Chapter 4

Numerical solution of highly non-linear fractional order reaction advection diffusion equation using cubic B-spline collocation method

4.1 Introduction

In recent years during the literature survey, the intensive study on fractional differential equations are found due to its major applications in physical, biological, geological, and financial systems. For example, a random walk model is successfully modeled by Gorenflo and Mainardi [134], Del-Castillo-Negrete et al. [135] have modeled fractional diffusion equation to describe non-diffusive transport in plasma turbulence and Gerolymatou and [136] have developed a non-linear fractional diffusion model for capillary flow through porous media. The mathematical descriptions of the diffusion equation have a long history. The fractional-order diffusion model of a particular phenomenon depends on various terms, viz., a phenomenological model is based on conservation of mass and constitutive law; the probabilistic model is based on a random walk and central limit theorem, etc. The fractional diffusion model in porous media has significant applications in ground water contamination problem. Several examples of porous media in the form of fractional order diffusion model can be found in literature like Deans [137] has developed a mathematical model for dispersion in the direction of flow in porous media. Mualem [111] have given a model for predicting the hydraulic conductivity of unsaturated porous media, Feng

[138] developed a model on compressible miscible displacement in porous media, Khaled and Vafai [139] have given a porous media model for flow and heat transfer in biological tissues. Choquet [140] have developed a model on compressible displacement in porous media. Fractional order reaction advection diffusion equation(FRADE) is mainly of the following form

$$ {}_0^C D_t^\alpha u = \frac{\partial}{\partial x}\left(A(u)\frac{\partial u}{\partial x}\right) + B(u)\frac{\partial u}{\partial x} + C(u), \quad 0 < \alpha < 1, $$

where, $A(u), B(u), C(u)$ are smooth functions. This model helps to describe various type of physical, biological and ecological processes [141, 142, 143, 144, 145]. In this chapter, the author will deal with the FRADE as

$$ {}_0^C D_t^\alpha u(x,t) = \frac{\partial}{\partial x}\{u^l(x,t)\frac{\partial u(x,t)}{\partial x}\} - v\frac{\partial u(x,t)}{\partial x} + Ku(x,t)(1-u(x,t)), \quad 0 < \alpha < 1, \quad (4.1) $$

where

$$ {}_0^C D_t^\alpha f(t) = \frac{1}{\Gamma(n-\alpha)}\int_0^t (t-\tau)^{(n-\alpha-1)} f^{(n)}(\tau)d\tau, \quad \alpha > 0, \tau > 0, $$

is the Caputo fractional-order derivative of $f(t)$ [41] for $0 < \alpha < 1$, v is the advection coefficient, K is the reaction coefficient and $l \in I^+$ is the degree of nonlinearity in diffusive term. $u(x,t)$ denotes the concentration of solute in the fluid at time t, and at a distance x, v represents the velocity of the fluid. For conservative system the reaction term coefficient $K = 0$ and for non-conservative system $K \neq 0$. The equation (4.1) is solved using the following prescribed initial and boundary conditions given as

$$ \begin{aligned} u(x,0) &= g_1(x) \;\; 0 \le x \le 1, \\ u(0,t) &= g_2(t) \;\; 0 < t \le 1, \\ u(1,t) &= g_3(t) \;\; 0 < t \le 1. \end{aligned} \quad (4.2) $$

The above diffusive model can physically be represented as the solute is getting diffused in any kind of fluid to the lower concentration like salt in water etc.

As analytic solutions of the FRADEs are available only for few simple cases, therefore developing very accurate and efficient numerical methods is of great interest. Many numerical methods have been developed to solve differential equations of fractional order, for example, finite difference method(FDM) [79], finite element method(FEM) [146], and homotopy perturbation method(HPM) [117] to solve fractional order diffusion equation. Rose [147] have solved the diffusion equation with compact finite volume method, Zhang and Chen [148] solved the diffusion equation with weak Galerkin finite element method, Zhang et al. [149] developed an approximate scheme to solve diffusion equation, Polyanin [150]

have solved the diffusion equation with variable coefficient and Fairweather et al. [151] have used an orthogonal spline collocation method to solve the two-dimensional fractional diffusion-wave equation. Hajipour et al. [152] have solved the variable order diffusion equation with accurate discretization. Kanwal et al. [153] have solved fractional diffusion wave equation and fractional Klein–Gordon equation with the help of two-dimensional Genocchi polynomials. Zhang et al. [154] have solved the fourth order diffusion equation with the help of spline collocation method. In the present chapter, Cubic B-spline collocation method has been used to solve the proposed model. Spline functions especially B-Spline functions are very powerful tools to approximate the numerical solution of partial differential equations [155, 156] because those are piecewise continuous with small compact support. During the literature survey the author have gone through the numerical schemes given in [157, 158, 159, 160, 161, 162].

Crank-Nicolson scheme has been developed with the help of a cubic B-spline function to solve the proposed model. The Crank-Nicolson scheme is the combination of the forward Euler method at n and the backward Euler method at $(n+1)$ points. The main aim of this chapter is to discuss the variations of the solute concentration due to the effect of the increase in the degree of non-linearity in diffusive term and also due to the variations of fractional order time derivative.

In order to obtain the numerical solution of the proposed method we need a finite scheme for the fractional-order time derivative of solute concentration. $L1$ formula is derived to discretize the Caputo's derivative. Now dividing the time domain in N equal parts as $t_n = n\Delta t$ for $0 \leq n \leq N-1$. As fractional-order time derivative α of model (4.1) is bounded between $(0,1)$, hence Caputo fractional-order derivative can be written as

$$\begin{aligned}
{}_0^C D_t^\alpha f(t) &= \frac{1}{\Gamma(1-\alpha)} \int_0^t (t-\eta)^\alpha \frac{df(\eta)}{d\eta} d\eta \\
&= \frac{1}{\Gamma(1-\alpha)} \int_0^t \frac{1}{\eta^\alpha} \frac{df(t-\eta)}{d\eta} d\eta \\
{}_0^C D_t^\alpha f(t)\big|_{t_n} &= \frac{1}{\Gamma(1-\alpha)} \sum_{k=0}^{n-1} \int_{k\Delta t}^{(k+1)\Delta t} \frac{1}{\eta^\alpha} \frac{d}{d\eta} f(t_m - \eta) d\eta \\
&= \frac{1}{\Gamma(1-\alpha)} \sum_{k=0}^{n-1} \frac{f(t_m - k\Delta t) - f(t_m - (k+1)\Delta t)}{\Delta t} \int_{k\Delta t}^{(k+1)\Delta t} \frac{1}{\eta^\alpha} d\eta
\end{aligned}$$

$$ {}_0^C D_t^\alpha f(t)\big|_{t_n} = \frac{(\Delta t)^{-\alpha}}{\Gamma(2-\alpha)} \sum_{k=0}^{n-1} b_k^\alpha [f(t_{n-k}) - f(t_{n-1-k})] + o((\Delta t)^{2-\alpha}), \tag{4.3}$$

where

$$b_k^\alpha = (k+1)^{1-\alpha} - k^{1-\alpha}.$$

The remaining portions of the chapter are given as follows. Section (4.2) consists of basic definitions. In section (4.3), the numerical scheme has been developed with the help of Cubic B-spline. The stability and convergence of the scheme have been discussed in sections (4.5) and (4.6), respectively. In section (4.7), the derived scheme is applied in four particular cases of the proposed model and compared their analytical and numerical results through l^2-norm and l^∞-norm. In section (4.8), the proposed method has been applied on the considered mathematical model and the effects on solute profile due to increase in the non-linearity in diffusive term for different fractional-order time derivatives are discussed. Overall work is concluded in section (4.9).

4.2 Description of the Cubic B-spline function

To solve the proposed model (4.1) with the initial and boundary conditions (4.2), it is needed to define the cubic B-spline base functions. The interval $[a, b]$ has been partitioned in N finite equal lengths having knots x_m, $m = 0, 1, 2, ..., N$ s. t. $a = x_0 < x_1 < x_2 < ... < x_N = b$ with $h = x_{m+1} - x_m$. Cubic B-spline function $\psi_m(x)$ is defined below at the knots x_m over the interval $[a, b]$ as

$$\psi_m = \frac{1}{h^3}\begin{cases} (x - x_{m-2})^3, & x \in [x_{m-2}, x_{m-1}], \\ h^3 + 3h^2(x - x_{m-1}) + 3h(x - x_{m-1})^2 - 3(x - x_{m-1}), & x \in [x_{m-1}, x_m], \\ h^3 + 3h^2(x_{m+1} - x) + 3h(x_{m+1} - x)^2 - 3(x_{m+1} - x)^3, & x \in [x_m, x_{m+1}] \\ (x_{m+2} - x)^3, & x \in [x_{m+1}, x_{m+2}], \\ 0, & otherwise. \end{cases}$$

The set of spline functions $\{\psi_{-1}(x), \psi_0(x), \psi_1(x), ..., \psi_{N+1}(x)\}$ form a basis for the function defined over $[a, b]$. Now the approximate solution $U_N(x, t)$ of the problem can be expressed in terms of basis function as

$$U_N(x, t) = \sum_{m=-1}^{N+1} \delta_m(t)\psi_m(x), \tag{4.4}$$

where δ_m's are the time dependent unknown quantities which are to be determined. Each cubic B-spline covers four elements, so that an element is covered by four cubic B-splines and each cubic B-spline vanishes outside the interval $[x_{m-2}, x_{m+2}]$. Using the above approximations, the values of U_m, U'_m and U''_m i.e., the values of the solution of $U(x, t)$ at

the node x_m will be

$$\begin{aligned} U_m &= U(x_m) = \delta_{m-1}(t) + 4\delta_m(t) + \delta_{m+1}(t), \\ U'_m &= U'(x_m) = \frac{3}{h}(-\delta_{m-1}(t) + \delta_{m+1}(t)), \\ U''_m &= U''(x_m) = \frac{6}{h^2}(\delta_{m-1}(t) - 2\delta_m(t) + \delta_{m+1}(t)). \end{aligned} \tag{4.5}$$

4.3 Description of the method

In this section, an unconditionally stable scheme is developed for the considered model (4.1) with the help of Cubic B-spline method which is used to solve the considered problem together with the initial and boundary conditions (4.2). As the problem is non-linear, so during use of Crank-Nicolson formula, let us linearize the non-linear terms by using Taylor's series. Now on discretizing the equation (4.1) and using Crank-Nicolson formula, we get

$$\begin{aligned} \left({}_0^C D_t^\alpha u(x,t)\right)_m^{n+1} &= \frac{F_m^{n+1} + F_m^n}{2}, \\ where\ \ F_m^n &= \left(\frac{\partial}{\partial x}\{u^l(x,t)\frac{\partial u(x,t)}{\partial x}\} - v\frac{\partial u(x,t)}{\partial x} + Ku(x,t)(1-u(x,t))\right)_m^n, \end{aligned} \tag{4.6}$$

$$\begin{aligned} (u^l)_m^{n+1}(u_{xx})_m^{n+1} &= l(u^{l-1})_m^n(u_{xx})_m^n(u)_m^{n+1} + (u^l)_m^n(u_{xx})_m^{n+1} - l(u^l)_m^n(u_{xx})_m^n \\ (u^{l-1})_m^{n+1}(u_x^2)_m^{n+1} &= (l-1)(u^{l-2})_m^n(u_x^2)_m^n u_m^{n+1} + 2(u^{l-1})_m^n(u_x)_m^n(u_x)_m^{n+1} \\ &\quad - l(u^{l-1})_m^{n+1}(u_x^2)_m^{n+1}, \\ (u^2)_m^{n+1} &= 2u_m^n u_m^{n+1} - (u^2)_m^n. \end{aligned} \tag{4.7}$$

Equation (4.6) with the use of equation (4.7) gives

$$a_1\delta_{m-1}^{n+1} + a_2\delta_m^{n+1} + a_3\delta_{m+1}^{n+1} = \rho_m^n \tag{4.8}$$

At every time level for the values of $m = 0, 1, 2, ..., N$, we get a system of linear algebraic $(N+1)$ equations with $(N+3)$ unknowns. Now to obtain the unique solution we need two more equations. We can use boundary conditions (4.2) to get the extra equations as follows

$$\begin{aligned} \delta_{-1}^{n+1} + 4\delta_0^{n+1} + \delta_1^{n+1} &= g_2[(n+1)\Delta t], \\ \delta_{N-1}^{n+1} + 4\delta_N^{n+1} + \delta_{N+1}^{n+1} &= g_3[(n+1)\Delta t]. \end{aligned} \tag{4.9}$$

With the aid of above two equations we will have the $(N+3)$ algebraic equations with $(N+3)$ unknowns. On representing these equations in terms of coefficient matrix, we will

get a matrix A of $(N+3)\times(N+3)$ order so that

$$AC = \rho, \tag{4.10}$$

where

$$A = \begin{pmatrix} 1 & 4 & 1 & 0 & 0\cdots & 0 & 0 & 0 \\ a_1 & a_2 & a_3 & 0 & 0\cdots & 0 & 0 & 0 \\ 0 & a_1 & a_2 & a_3 & 0\cdots & 0 & 0 & 0 \\ \vdots & \vdots & \vdots & \vdots & \vdots\ddots & \vdots & \vdots & \vdots \\ 0 & 0 & 0 & 0 & 0\cdots & a_1 & a_2 & a_3 \\ 0 & 0 & 0 & 0 & 0\cdots & 1 & 4 & 1 \end{pmatrix}_{(N+3)\times(N+3)},$$

and

$$C = (\delta_{-1}^{n+1}, \delta_0^{n+1}, \delta_1^{n+1}, ..., \delta_{N+1}^{n+1})^T,$$
$$\rho = (g_2[(n+1)\Delta t], \rho_0^n, \rho_1^n, ...\rho_N^n, g_3[(1+n)\Delta t])^T,$$

with

$$\begin{aligned}
a_1 &= [2B - \frac{6l}{h^2}(\delta_{m-1}^n + 4\delta_m^n + \delta_{m+1}^n)^{l-1}(\delta_{m-1}^n - 2\delta_m^n + \delta_{m+1}^n) - \frac{6}{h^2}(\delta_{m-1}^n + 4\delta_m^n + \delta_{m+1}^n)^l \\
&\quad - \frac{9l(l-1)}{h^2}(\delta_{m-1}^n + 4\delta_m^n + \delta_{m+1}^n)^{l-2}(-\delta_{m-1}^n + \delta_{m+1}^n)^2 + \frac{18l}{h^2}(\delta_{m-1}^n + 4\delta_m^n + \delta_{m+1}^n)^{l-1}(-\delta_{m-1}^n + \delta_{m+1}^n) \\
&\quad - \frac{3v}{h} - K - 2K(\delta_{m-1}^n + 4\delta_m^n + \delta_{m+1}^n)], \\
a_2 &= [8B - \frac{24l}{h^2}(\delta_{m-1}^n + 4\delta_m^n + \delta_{m+1}^n)^{l-1}(\delta_{m-1}^n - 2\delta_m^n + \delta_{m+1}^n) + \frac{12}{h^2}(\delta_{m-1}^n + 4\delta_m^n + \delta_{m+1}^n)^l \\
&\quad \frac{36l(l-1)}{h^2}(\delta_{m-1}^n + 4\delta_m^n + \delta_{m+1}^n)^{l-2}(-\delta_{m-1}^n + \delta_{m+1}^n)^2 - 4K + 8K(\delta_{m-1}^n + 4\delta_m^n + \delta_{m+1}^n)], \\
a_3 &= [2B - \frac{6l}{h^2}(\delta_{m-1}^n + 4\delta_m^n + \delta_{m+1}^n)^{l-1}(\delta_{m-1}^n - 2\delta_m^n + \delta_{m+1}^n) - \frac{6}{h^2}(\delta_{m-1}^n + 4\delta_m^n + \delta_{m+1}^n)^l \\
&\quad - \frac{9l(l-1)}{h^2}(\delta_{m-1}^n + 4\delta_m^n + \delta_{m+1}^n)^{l-2}(-\delta_{m-1}^n + \delta_{m+1}^n)^2 - \frac{18}{h^2}(\delta_{m-1}^n + 4\delta_m^n + \delta_{m+1}^n)^{l-1}(-\delta_{m-1}^n + \delta_{m+1}^n) \\
&\quad + \frac{3v}{h} - K + 2K(\delta_{m-1}^n + 4\delta_m^n + \delta_{m+1}^n)], \\
\rho_m^n &= 2l(\delta_{m-1}^n + 4\delta_m^n + \delta_{m+1}^n) + \frac{6(1-l)}{h^2}(\delta_{m-1}^n + 4\delta_m^n + \delta_{m+1}^n)^l(\delta_{m-1}^n - 2\delta_m^n + \delta_{m+1}^n) \\
&\quad + \frac{9l(1-l)}{h^2}(\delta_{m-1}^n + 4\delta_m^n + \delta_{m+1}^n)^{l-1}(-\delta_{m-1}^n + +\delta_{m+1}^n)^2 - \frac{3v}{h}(-\delta_{m-1}^n + \delta_{m+1}^n) \\
&\quad + K(\delta_{m-1}^n + 4\delta_m^n + \delta_{m+1}^n) \\
&\quad - 2B\sum_{k=1}^{n}[(k+1)^{1-\alpha} - k^{1-\alpha}](\delta_{m-1}^{n+1-k} - \delta_{m-1}^{n-k} + 4\delta_m^{n+1-k} - 4\delta_m^{n-k} + \delta_{m+1}^{n+1-k} - \delta_{m+1}^{n-k}),
\end{aligned}$$

and

$$B = \frac{(\Delta t)^{-\alpha}}{\Gamma(2-\alpha)}.$$

From equations (4.9), we can say that unknown weights C depend on the unknown weights of previous time levels. Hence we first need the values of unknown weights C at the initial time level.

4.4 Initial State

In this section the values of unknown weights δ are found at the initial time level. The initial vector $c^0 = (\delta^0_{-1}, \delta^0_0, \delta^0_1, ..., \delta^0_{N+1})$ is determined by initial condition (4.2) and its derivatives on initial and boundary points as

$$\begin{aligned} u(x,0) &= g_1(x), \\ u_{xx}(0,0) &= \frac{d^2 g_1(x)}{dx^2}|_{x=0}, \\ u_{xx}(1,0) &= \frac{d^2 g_1(x)}{dx^2}|_{x=1}. \end{aligned}$$

On discretizing above equations, we get

$$\begin{aligned} \frac{6}{h^2}(\delta^0_{m-1} + 4\delta^0_m + \delta^0_{m+1}) &= g_1(mh), \\ \frac{6}{h^2}(\delta^0_{-1} - 2\delta^0_0 + \delta^0_1) &= \frac{d^2 g_1(x)}{dx^2}|_{x=0}, \\ \frac{6}{h^2}(\delta^0_{N-1} - 2\delta^0_N + \delta^0_{N+1}) &= \frac{d^2 g_1(x)}{dx^2}|_{x=1}. \end{aligned} \tag{4.11}$$

Since equation (4.10) contains $(N+3)\times(N+3)$ equations with $(N+3)\times(N+3)$ unknowns, therefore we get

$$A^0 C^0 = \rho^0, \tag{4.12}$$

where

$$A^0 = \begin{pmatrix} 1 & -2 & 1 & 0\cdots & 0 & 0 & 0 \\ 1 & 4 & 1 & 0\cdots & 0 & 0 & 0 \\ 0 & 1 & 4 & 1\cdots & 0 & 0 & 0 \\ \vdots & \vdots & \vdots & \vdots\ddots & \vdots & \vdots & \vdots \\ 0 & 0 & 0 & 0\cdots & 1 & 4 & 1 \\ 0 & 0 & 0 & 0\cdots & 1 & -2 & 1 \end{pmatrix}$$

and

$$C^0 = (\delta^0_{-1}, \delta^0_0, \delta^0_1, ..., \delta^0_{N+1})^T,$$
$$\rho^0 = (\frac{d^2 g_1(x)}{dx^2}|_{x=0}, g_1(0), g_1(h), g_1(2h), ..., g_1(Nh), \frac{d^2 g_1(x)}{dx^2}|_{x=1})^T.$$

Hence from equations (4.9) and (4.11), the values of unknown weights are found at the required time levels and after putting the values of these unknowns in the equation (4.4), the approximate solution will be obtained.

4.5 Stability Analysis

In this section the Fourier method is discussed to investigate the stability of the scheme (4.8). The concept of stability is associated with the concept of boundedness of computation errors. As the concerned FRADE is nonlinear, to investigate the stability of proposed scheme by Fourier method, let us consider that the product term is locally constant as u^l=τ where τ is taken as local constant [163, 164]. The scheme (4.6) is described as

$$2({}^C_0 D^\alpha_t u) = \tau[(u_{xx})^{n+1}_m + (u_{xx})^n_m] - v[(u_x)^{n+1}_m + (u_x)^n_m] + K(1-\tau)[u^{n+1}_m + u^n_m]. \quad (4.13)$$

Consider u^n_m and $\widetilde{u^n_m}$ be the exact and actual computed solutions of the problem respectively. Then the error term is defined as

$$\eta^n_m = u^n_m - \widetilde{u^n_m}, \text{ where the vector } \eta^n = \{\eta^n_0, \eta^n_1, ..., \eta^n_N\}.$$

η^n_m satisfies the scheme obtained by equation (4.13). Rewriting the equation (4.13) after substituting $\eta^n_m = \xi^n e^{im\phi}$, where ϕ=ωh, ω is a wave number, ξ^n is Fourier coefficient at time level n and $i = \sqrt{-1}$, we finally get

$$\xi^{n+1} = \frac{p_1}{p_2}\xi^n - \frac{2B}{p_2}\sum_{k=1}^{n}[(k+1)^{1-\alpha} - (k)^{1-\alpha}][\xi^{n+-k} - \xi^{n-k}](2cos\phi + 4), \quad (4.14)$$

where

$$p_1 = 2B(2cos\phi + 4) + \frac{6\tau}{h^2}(2cos\phi) + K(1-\tau)(2cos\phi + 4) - \frac{6vi}{h}sin\phi,$$
$$p_2 = 2B(2cos\phi + 4) - \frac{6\tau}{h^2}(2cos\phi) - K(1-\tau)(2cos\phi + 4) + \frac{6vi}{h}sin\phi.$$

Since the wave number $\omega = 2\pi/\lambda$, where λ is the wave length, so ϕ=ωh= 2π/N for $0 < \phi < N$.

$$|p_1| - |p_2| = \frac{-96B\tau}{h^2}(2cos\phi + 4)sin^2\phi + 8K(1-\tau)B(2cos\phi + 4)^2 < 0 \tag{4.15}$$

Hence from the above equation (4.15), we may conclude that $|\frac{p_1}{p_2}| < 1$.

4.5.1 Proposition

Suppose that ξ^n, $n = 1, 2, ..., N+1$ is the solution of equation (4.14), then we have

$$|\xi^n| \leq |\xi^0|, \quad n = 1, 2, .., N+1. \tag{4.16}$$

Proof: The mathematical induction is applied to verify inequality (4.16). If we put $n = 0$ in equation (4.14), we get

$$|\xi^1| = |\frac{p_1}{p_2}||\xi^0| \leq |\xi^0|, \quad \text{as} \quad |\frac{p_1}{p_2}| < 1.$$

Now suppose that $|\xi^n| \leq |\xi^0|$ for $n = 1, 2, ..., N$. Then from equation (4.14), we get

$$\begin{aligned}
|\xi^{n+1}| &\leq |\frac{p_1}{p_2}||\xi^n| + \frac{2B(2cos\phi + 4)b_n}{|p_2|}|\xi^0| + \frac{2B(2cos\phi + 4)b_1}{|p_2|}|\xi^n| \\
&\qquad + \frac{2B(2cos\phi + 4)}{|p_2|}\sum_{k=1}^{n-1}(b_k - b_{k+1})|\xi^{n-k}| \\
&\leq \{\frac{|p_1| + 4Bb_1(2cos\phi + 4)}{|p_2|}\}|\xi^0| \\
&\leq |\xi^0|,
\end{aligned}$$

which shows the meaningful completion of the mathematical induction.

Theorem 1. The scheme (4.8) is unconditionally stable.

Proof:

$$||u^n - \widetilde{u^n}||_{l_2}^2 = ||\eta^n||_{l_2}^2 = h\sum_{m=0}^{N} |\xi^n e^{im\phi}|^2$$
$$\leq h\sum_{k=0}^{N} |\xi^0 e^{im\phi}|$$
$$\text{i.e., } \leq ||\eta^0||_{l_2}^2$$
$$\text{i.e., } \leq ||u^0 - \widetilde{u^0}||_{l_2}^2.$$

Thus it is seen from above theorem that the error of this method at any time level n does not grow and is bounded by the initial error. So the method is unconditionally stable. The term unconditionally stable means that it is not necessary to impose any particular restriction on the developed scheme to prove the stability of the scheme.

4.6 Convergence Analysis

In this section the convergence of proposed method is examined. Before starting the convergence analysis we need certain results which are stated bellow.

Theorem 2. Suppose that $f(x) \in C^4[0,1]$ and $|f^4(x)| \leq L$, $\forall x \in [0,1]$ and $\triangle = \{0 = x_0 < x_1 < x_2 < .... < x_N = 1\}$ be the equally spaced partition of $[0,1]$ with step size h. If $S_{\triangle}(x)$ is unique spline function that interpolates $f(x)$ at nodes $x_0, x_1, x_2, ..., x_N \in \triangle$, then there exists a constant $\lambda_j \leq 2$, such that

$$||f^j(x) - S_{\triangle}^j(x)||_{\infty} \leq \lambda_j L h^{4-j}, \ \ \forall x \in [0,1], \tag{4.17}$$

where $j = 0, 1, 2, 3$ and $||.||_{\infty}$ is ∞-norm.

Proof. For the proof see, p.105 of [165].

4.6.1 Lemma

The B-splines $\psi_{-1}, \psi_0, ..., \psi_{N+1}$ satisfy the following inequality

$$|\sum_{m=-1}^{N+1} \psi_m| \leq 10, \quad 0 \leq x \leq 1. \tag{4.18}$$

The proof of the Lemma can be found in Kadalbajoo et al. [166].

Theorem 3. If $U(x,t)$ is the cubic B-spline collocation approximation to the exact solution $u(x,t)$, then

$$||u(x,t^n) - U(x,t^n)||_\infty = \omega + h^2,$$

where $k = \triangle t$ and $h = x_{i+1} - x_i$.

Proof: Consider $u(x,t)$ be the exact solution of the proposed problem (4.1) with the conditions (4.2) and $U(x,t) = \sum_{m=-1}^{N+1} \delta_m \psi_m(x)$ be the B-spline collocation approximation of $u(x,t)$. Again consider $\widetilde{U}(x,t) = \sum_{m=-1}^{N+1} \widetilde{\delta}_m \psi_m(x)$ is solution of the problem calculated due to some computational errors. To estimate the error $||u(x,t) - U(x,t)||_\infty$, we estimate $||u(x,t) - \widetilde{U}(x,t)||_\infty$ and $||\widetilde{U}(x,t) - U(x,t)||_\infty$ separately. From $U(x,t)$ and $\widetilde{U}(x,t)$, we get $AC = \rho$ and $A\widetilde{C} = \widetilde{\rho}$. From these two equations we have $A(C - \widetilde{C}) = \rho - \widetilde{\rho}$. Now we will estimate the bound for $||\rho - \widetilde{\rho}||_\infty$, where $\widetilde{\rho} = (g_2[(n+1)\triangle t], \widetilde{\rho}_0^n, \widetilde{\rho}_1^n, \widetilde{\rho}_3^n ... \widetilde{\rho}_N^n, g_3[(n+1)\triangle t])$ and

$$\begin{aligned}\widetilde{\rho}_m^n = {} & 2B\widetilde{U}_m^n + (1-l)(\widetilde{U}^l)_m^n + (1-l)(\widetilde{U}^l - 1)_m^n (\widetilde{U}_x^2)_m^n - v(\widetilde{U}_x)_m^n \\ & + K\widetilde{U}_m^n - 2B\sum_{k=1}^{n}[(k+1)^\alpha - k^\alpha](\widetilde{U}_m^{n+1-k} - \widetilde{U}_m^{n-k}).\end{aligned}$$

By using Theorem 2 and [167] (page 218), we obtain

$$\begin{aligned}||\rho - \widetilde{\rho}||_\infty &\leq M(|U(x) - \widetilde{U}(x)| + |U' - \widetilde{U}'| + |U'' - \widetilde{U}''|) \\ &\leq ML\lambda_0 h^4 + ML\lambda_1 h^3 + ML\lambda_2 h^2.\end{aligned}$$

The above inequality can be written in the form

$$||\rho - \widetilde{\rho}||_\infty \leq M_1 h^2, \tag{4.19}$$

where $M_1 = ML\lambda_0 h^2 + ML\lambda_1 h + ML\lambda_2$. Now on taking infinity norm on the equation $(C - \widetilde{C}) = A^{-1}(\rho - \widetilde{\rho})$ on both sides and using equation (4.19), we have

$$||C - \widetilde{C}||_\infty \leq ||A^{-1}||_\infty ||\rho - \widetilde{\rho}||_\infty \leq M_2 h^2, \tag{4.20}$$

where $M_2 = M_1 ||A^{-1}||_\infty$. Now using the lemma 5.1, we get

$$||U(x) - \widetilde{U}(x)||_\infty = ||\sum_{m=-1}^{N+1} (\delta_m - \widetilde{\delta}_m)\psi_m||_\infty \leq ||\delta_m - \widetilde{\delta}_m||_\infty |\sum_{k=-1}^{N+1} \psi_m| = 10M_2 h^2. \tag{4.21}$$

Now the error of this method will be

$$||u(x,t^n) - U(x,t^n)||_\infty \leq ||u(x,t^n) - \widetilde{U}(x,t^n)||_\infty + ||\widetilde{U}(x,t^n) - U(x,t^n)||_\infty.$$

With the aid of equation (4.21) and Theorem 2, the above inequality is reduced to

$$||u(x,t^n) - U(x,t^n)||_\infty \leq \lambda_0 L h^4 + 10 M_2 h^2 = \omega h^2, \tag{4.22}$$

where $\omega = \lambda_0 L h^2 + 10 M_2$. Hence order of convergence of our method is $O(h^2)$.

4.7 Numerical Examples

In this section, the proposed scheme given in section (4.3) is applied on four different numerical problems, which are the particular cases of concerned mathematical model (4.1) with the prescribed conditions (4.2) and compare the obtained numerical results with the existing exact solutions. The computing errors are measured by l^2 and l^∞-norms as

$$||u(x,t_n) - U(x,t_n)||_{l^2} = \sqrt{h \sum_{m=0}^{N} |u(x_m,t_n) - U(x_m,t_n)|^2},$$
$$||u(x,t_n) - U(x,t_n)||_{l^\infty} = \max_{0 \leq m \leq N} |u(x_m,t_n)|.$$

In all examples discussed here, $u(x,t)$ represents the exact solution of the example and $U(x,t)$ represents the numerical solution obtained by the proposed method. To estimate the order of convergence of the method numerically, we use the following log ratio formula as

$$p = \frac{log(||e||_\infty(N_{i+1})) - log(||e||_\infty(N_1))}{log(N_i - log(N_{i+1}))},$$

where $||e||_\infty(N_i)$ is error at the number of partitioning N_i.

Example 1.

Now to evaluate the accuracy and efficiency of the proposed numerical method, the numerical solution obtained by the proposed method is compared with the exact solution of the concerned problem for the integer order ($\alpha = 1$). The exact solution of the mathematical problem (4.1) with initial and boundary conditions (4.2) for $l = 1$, $K = 0$ and $v = 0$ i.e., in the absence of reaction and advection terms is $u(x,t) = x + t$ [117]. After solving for

$h = \frac{1}{4}$ and $\Delta t = \frac{1}{4}$, the absolute errors found for various values of x and t are given in Table 4.1.

TABLE 4.1: Comparison of results for Example 1.

t	x	Approximate Solution	Exact Solution	Absolute Error
0.5	0.25	0.750	0.750	2.22045×10^{-16}
	0.50	1.0	1.0	2.22045×10^{-16}
	0.5	1.25	1.25	$6.66134 \times 10^{-}16$
	1.0	1.50	1.50	0.00
0.75	0.25	1.0	1.0	2.22045×10^{-16}
	0.50	1.25	1.25	4.44089×10^{-16}
	0.75	1.50	1.50	1.11022×10^{-15}
	1.0	1.75	1.75	0.00

It is clear from the tabular representation that the proposed method is very efficient. For very small values of h and Δt, the absolute error is very less.

Example 2.

The proposed method is applied to a second problem and compare the results with exact solution. On choosing $l = 0$, $v = 1$ and $K = 0$ in the integer order (α=1) form of the proposed model (4.1), it is seen that the problem with prescribed initial and Drichlet boundary conditions, has the exact solution given as [168].

$$u(x,t) = \frac{1}{\sqrt{1+200t}} exp[\frac{-50(x-t)^2}{1+200t}]. \tag{4.23}$$

The l^2 and l^∞ errors between numerical values and the exact values are depicted in Table 4.2 for $N = 10$ at $t = 0.5$.

TABLE 4.2: Calculated error of approximate solution in l^2 and l^∞-norms for Example 2.

Δt	$\|\|u-u_N\|\|_{l^2}$	Convergence rate	$\|\|u-u_N\|\|_{l^\infty}$	Convergence rate
1/12	0.0156791	-	0.0400588	-
1/24	0.0036972	2.08434	0.0079132	2.33979
1/48	0.0001341	4.78419	0.0002476	4.99783
1/96	0.0000244	2.4591	0.0000351	2.81799

Example 3.

The considered mathematical model (4.1) after taking $l = 0$, $v = 0$ and $\alpha = 1$ is reduced to

$$\frac{\partial u(x,t)}{\partial t} = \frac{\partial^2 u(x,t)}{\partial x^2} + Ku(x,t)(1-u(x,t)),$$

which has exact solution $u(x,t) = \left[1 + exp(\sqrt{\frac{K}{6}}x - \frac{5K}{6}t)\right]^{-2}$ [169], with prescribed initial and boundary conditions which can be extracted from the exact solution. The problem has been solved with the proposed method for $N = 5$ and $\Delta t = 0.01$.

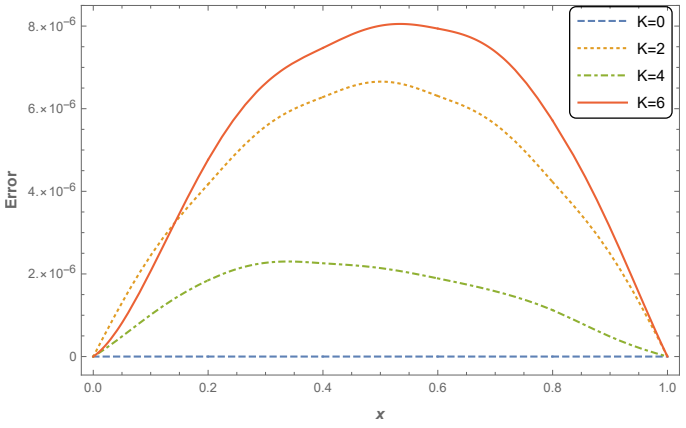

FIGURE 4.1: Plot of absolute error vs. x for different values of K at $t = 1$.

From the above Fig. 4.1, it is observed that proposed method is performing very efficiently even for very less temporal and spatial discretizations. Jebreen [169] has also solved this

problem for $K = 6$ and end-up with the best error of order $e - 5$, which clearly exhibits the better performance of our proposed method.

Example 4.

In the present example the proposed method is applied to solve the fractional order diffusion problem. Now taking $l = 0$, $v = 1$, $K = 0$ and adding one force term in the considered model (4.1), the problem will be transformed into the following form

$$ {}_0^C D_t^\alpha u(x,t) = \frac{\partial^2 u(x,t)}{\partial x^2} - \frac{\partial u(x,t)}{\partial x} + \frac{2t^{2-\alpha}}{\Gamma(3-\alpha)} + 2x - 2, \quad 0 < \alpha \leq 1. $$

With the prescribed initial and Drichlet Boundary conditions, the above problem has the exact solution as $u(x,t) = x^2 + t^2$ [170].

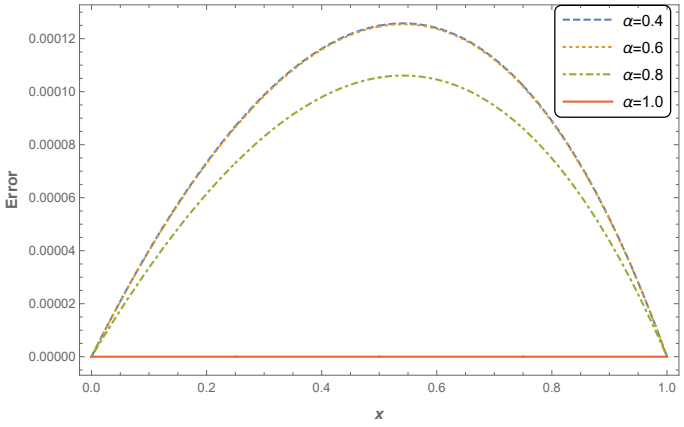

FIGURE 4.2: Plot of absolute error vs. x for different values of α at $t = 1$.

TABLE 4.3: Comparison of error obtained from Example 3 at $\alpha = 0.5$.

	Method [170] at $N = 51$, $\Delta t = 0.01$		Present Method at $N = 3$, $\Delta t = 0.01$	
t	L_∞	L_2	L_∞	L_2
0.1	6.086e-2	2.613e-1	6.080e-5	4.723e-5
0.5	2.958e-2	1.277e-1	1.610e-4	1.249e-4
1.0	2.114e-2	9.134e-2	2.372e-4	1.839e-4
1.5	1.732e-2	7.485e-2	2.959e-4	2.294e-4
2.0	1.503e-2	6.494e-2	3.454e-4	2.678e-4

From the above Table 4.3 it clear that the proposed method is performing better as compared to the method discussed in [170] in fractional order system. Fig. 4.2 shows the variations of the absolute error obtained for different values of α at $t = 1$.

Thus using the proposed numerical method on the four particular cases of the proposed model under the prescribed initial and boundary conditions, it may be concluded that the proposed method is very much accurate with a higher rate of convergence. After its validation, the derived scheme has been used to solve the FRADE (4.1).

4.8 Solution of the proposed FRADE model

In this section, the proposed mathematical model is solved with the following prescribed initial and boundary conditions as

$$\begin{aligned} u(x,0) &= 0, \\ u(0,t) &= 0.2, \\ u(1,t) &= 0, \end{aligned} \tag{4.24}$$

and determined the variations of the solute concentration $u(x,t)$ at $t = 0.5$ with the variations in nonlinearity terms exist in the diffusive term in the presence of the reaction term at different fractional order time derivative. The conditions (4.24) can be physically expressed as, the model is considered for a finite strip with initial value of the concentration of solute in the fluid is zero. At $x = 0$ there is a certain amount of solute present and at $x = 1$ it is zero in the fluid for a given time t.

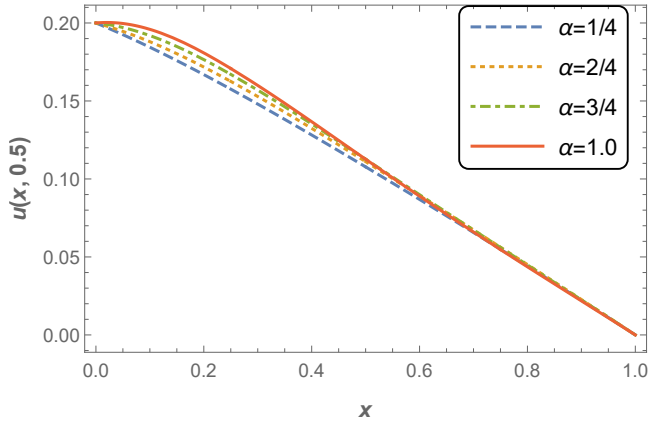

FIGURE 4.3: Plots of solute concentration vs. x for $K = 0.2$, $v = 0.2$, $l = 0$ at $t = 0.5$.

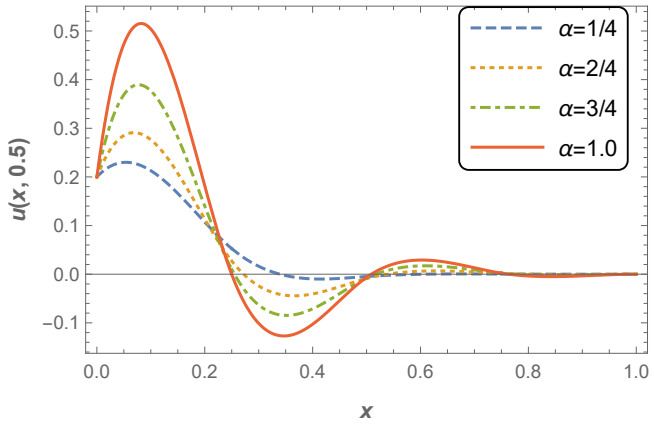

FIGURE 4.4: Plots of solute concentration vs. x for $K = 0.2$, $v = 0.2$, $l = 1$ at $t = 0.5$.

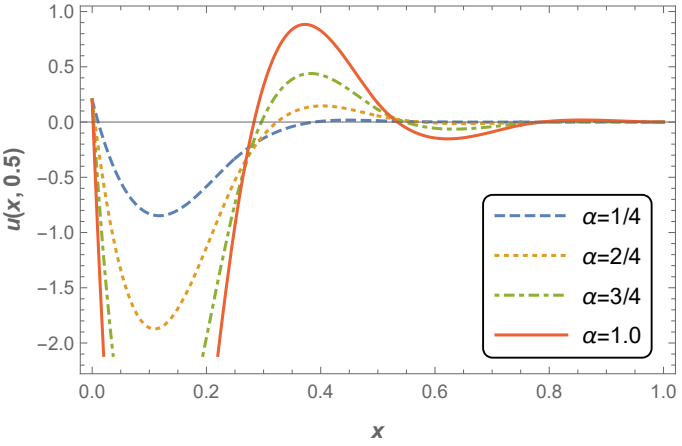

FIGURE 4.5: Plots of solute concentration vs. x for $K = 0.2$, $v = 0.2$, $l = 2$ at $t = 0.5$.

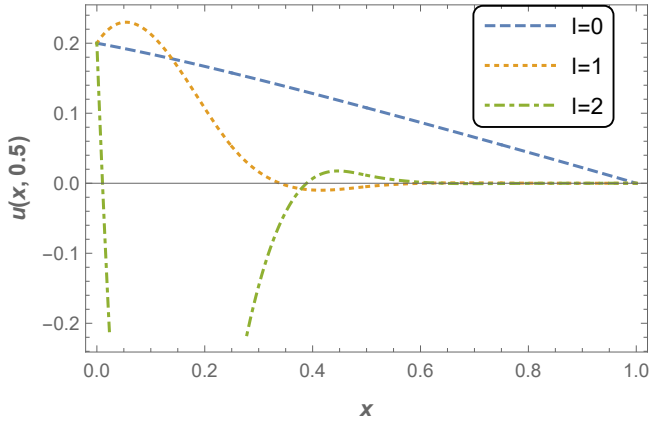

FIGURE 4.6: Plots of solute concentration vs. x for $\alpha = 0.25$, $K = 0.2$, $v = 0.2$, at $t = 0.5$.

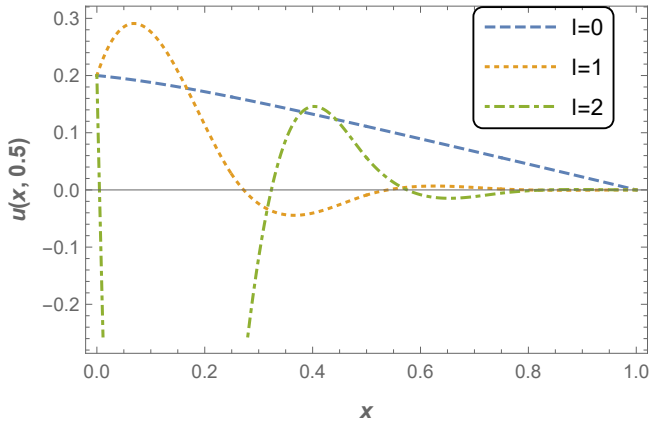

FIGURE 4.7: Plots of solute vs. x concentration for $\alpha = 0.5$, $K = 0.2$, $v = 0.2$, at $t = 0.5$.

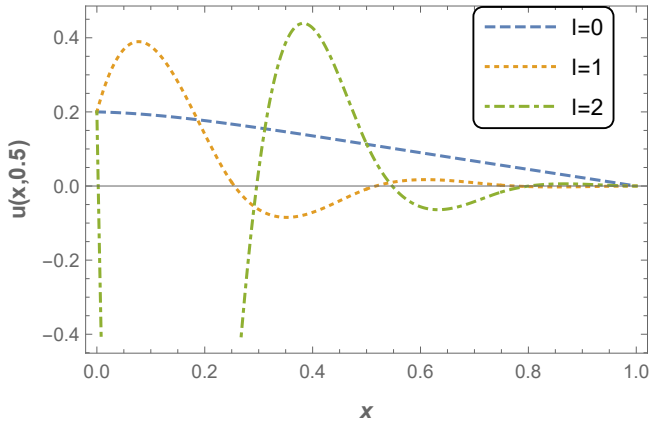

FIGURE 4.8: Plots of solute concentration vs. x for $\alpha = 0.75$, $K = 0.2$, $v = 0.2$, at $t = 0.5$.

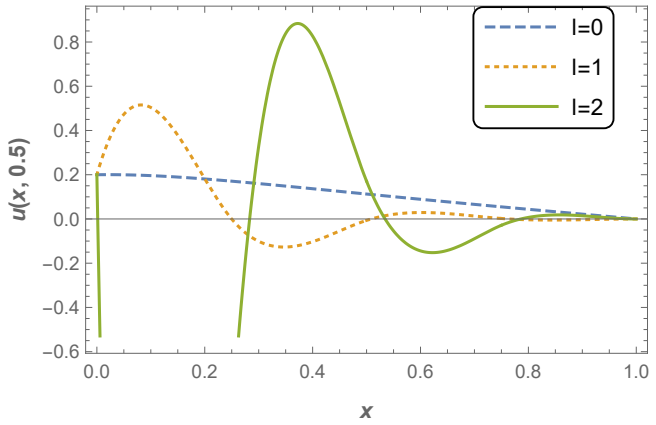

FIGURE 4.9: Plots of solute concentration vs. x for $\alpha = 1.0$, $K = 0.2$, $v = 0.2$, at $t = 0.5$.

Figs. 4.3-4.5 depict the effect on solute profile due to an increase in the order of rate of change of solute concentration with time for different values of l. From Fig. 4.3, it is observed that the solute profile increases with the increase in the order of time derivative. Figs 4.4 and 4.5 are drawn for $l = 1$ and $l = 2$, respectively. From these two figures, it is observed that there is a quick change in solute profile due to increase in the order of non-linearity of the diffusive term. It is also seen from the figures that the concentration increases in the positive sense due to a decrease in α. The negative solute concentration actually represents the back diffusion, which means the concentration of the solute is less than the concentration of the fluid. It is seen that as non-linearity increases, the nature of the solute profile is opposite, and the back diffusion will be higher. From Figs. 4.3-4.5, it is clear that solute concentration is decreasing to zero at the boundary of the domain $x = 1$ because we have considered in boundary condition that the solute concentration is zero at $x = 1$. On adding non-linearity in the diffusive term, we can observe a bulk increment in solute concentration rather than tending to zero, as in the case of $l = 0$. In order to observe the behavior of solute concentration due to the increase in the non-linearity in diffusive term, Figs. 4.6-4.9 have been plotted. These figures clearly show that as the non-linearity increases, overshoots of the concentration will be higher, and the curvature of the solute profile decreases.

4.9 Conclusion

In this chapter, a new scheme is developed to solve the FRADE with prescribed initial and boundary conditions based on cubic B-spline. It is shown that the derived scheme is

unconditionally stable and convergent. The developed scheme is applied in three particular cases of the proposed mathematical model in the integer-order system and one for fractional order system to validate the efficiency and accuracy of the scheme. The scheme is even accurate for fewer divisions of time and space domains. The salient feature of the chapter is to develop an efficient method, and observe the variations of solute concentration due to the effect of the order of non-linearity of the dispersion term in the presence of reaction term when the system approaches from integer-order to fractional order.